Analysis of three-dimensional photoacoustic imaging of a vascular tree *in vitro*

Magdalena C. Pilatou, Nico J. Voogd, Frits F. M. de Mul, et al.

View Online   Export Citation

ARTICLES YOU MAY BE INTERESTED IN

Analysis of three-dimensional photoacoustic imaging of a vascular tree *in vitro*

Magdalena C. Pilatou, Nico J. Voogd, Frits F. M. de Mul, and Wiendelt Steenbergen[a]
Biophysical Techniques Group, Department of Applied Physics, University of Twente, P.O. Box 217, 7500 AE Enschede, The Netherlands

Leon N. A. van Adrichem
Erasmus MC–University Medical Center Rotterdam, Department and Institute of Plastic and Reconstructive Surgery, Dr. Molewaterplein 60, 3015 GJ Rotterdam, The Netherlands

We used photoacoustics in order to image a vasculature cast, which was obtained from a Wistar rat. The main objective was to investigate the imaging quality and the performance of the beamforming algorithm. For these purposes, the specimen was measured in several Intralipid™ 10% solutions and it was scanned with scanning steps of 100, 200, and 300 μm. The measurements were performed with a disk-shaped detector, with PVDF as an active material and four fibers for the light delivery. From the recorded signals, three-dimensional images of the cast were constructed. © *2003 American Institute of Physics.* [DOI: 10.1063/1.1605491]

I. INTRODUCTION

The photoacoustic (PA) technique can be used to determine tissue characteristics,[1] to construct tomographic images of biological tissue,[2] or to monitor changes in the blood circulation.[3] The main advantage of it, compared to the existing optical imaging techniques (transillumination, optical coherence tomography, confocal microscopy, etc.), is that it does not suffer from the strong scattering of light in turbid media such as biological tissue. As a result of that, the penetration depth that can be reached is in the order of centimeters by using near-infrared light.

In medical ultrasonic imaging systems, images of interfaces between media with different acoustic impedances are constructed. The resolution is about 200 μm at 7 MHz signals. It was shown[4–7] that the PA technique makes it possible to image with 20 μm depth resolution. Furthermore, the light source can be tuned in different wavelengths (spectroscopy), which increases the selectivity of this technique compared to ultrasound.

Photoacoustic signal generation is generally the result of photothermal heating effects. The predominant mechanism in biological tissue is the process of thermal expansion, in which the absorption of light in a restricted volume is followed by thermal relaxation. The induced temperature increase produces a stress that propagates through the sample in all directions. For short laser pulses (<20 ns) this process can be considered as being adiabatic and the surrounding medium as noncompressible. The generated pressure is linearly proportional to the absorbed energy density and the PA pulse can be calculated analytically with the assumption that the temperature distribution is Gaussian. In that case, the shape of the transient of a spherical or a cylindrical source is a bipolar signal.[8–10] The transients from all acoustic sources can be measured by the detector elements, in the form of time-of-flight signals. These signals contain the information for the reconstruction of the positions of the sources.

For the construction of the sample three-dimensional (3D) image, a weighed delay and sum focused beam forming algorithm[10] is used. For each sample volume element to be imaged, the acoustic transit time to individual detectors is calculated. From that, the delays to be applied to these signals in order to construct a synthetic acoustic lens are calculated. The signals from the different detectors are delayed and weighted, a certain time window is applied and the signals are added for a specific focal point.

In general, the output of a phased array detector that is used for delay-and-sum beam forming can be expressed[11] as

$$S^f(t) = \frac{\sum_i^M w_i^f S_i(t + \delta_i^f)}{\sum_i^M w_i^f}, \qquad (1)$$

in which $S_i(t)$ is the signal from the ith receiver, $S^f(t)$ is the output of the beam former's sum for focus f, w_i^f is the amplitude weight factor (=directivity) for the detector i–focus f combination, δ_i^f is the time shift for the detector i–focus f combination, and M is the number of the detectors.

The w_i^f factors depend on the depth and the δ_i^f factors depend on the velocity of sound and the distance between the detector and the focus point. The algorithm performs a correction of the signal amplitude in order to optimize the signal-to-noise ratio (SNR). Besides that, a second correction using the time of flight is implemented in order to reduce the computing time.[7,12]

II. MATERIALS AND METHODS

We used PA in order to image a vasculature cast, which was obtained from a Wistar rat. The main objective was to investigate the imaging quality and the performance of the beam forming algorithm. For these purposes, the specimen was measured in several Intralipid™ 10% solutions and it
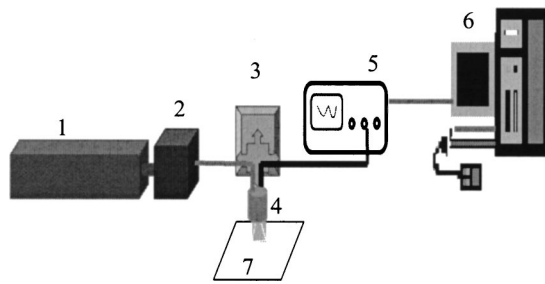
FIG. 1. Experimental setup. (1) Nd:YAG laser 532 nm at 50 Hz; (2) optics box, output 4 fibers; (3) $X-Y$ scanning system; (4) PA detector; (5) oscilloscope (Tektronix TDS 220) or Acqiris System; (6) PC for data processing; and (7) specimen position.

was scanned with scanning steps of 100, 200, and 300 μm. The cast was placed in several Intralipid™ dilutions and a volume of 7.5 mm×7.5 mm×5.6 mm was scanned. The specimen was measured in different depths, from 3 until 7 mm with a step size of 0.5 mm.

The experimental setup, which was used in the measurements, is shown schematically in Fig. 1. It consists of a disk-shaped piezoelectric sensor[5] with a diameter of 200 μm and PVDF film, 9 μm thickness, as the active material. For the light delivery, four fibers, each with a core diameter of 600 μm, were used. The fibers were integrated in the detector head and the measurements were carried out in "backward mode."[13]

As a light source, a Nd:YAG laser, frequency doubled (532 nm) with 14 ns pulses and a repetition rate of 50 Hz (LS 2139, Lotis TII) was used. The output energy of the fibers was 2.6 mJ/pulse and it was maintained below a 20 mJ/cm^2 pulse for all the experiments, which is the maximum permissible exposure for this type of laser pulses, according to the European regulations.

The sensor was positioned above the specimen, in Intralipid™ 10% dilution and the area of interest was scanned. The signal was collected and averaged by a 1 G sample/s, two-channel digital oscilloscope (TDS-220, Tektronix) and transferred to a computer for subsequent processing. The lateral resolution of the system is limited by the detector diameter and it is approximately 100–200 μm. The resolution in depth depends on the duration of the laser pulse and on the data acquisition system and it is about 10–20 μm.[4]

Specifically, a Wistar rat was perfused through the aorta with the two-component epoxy resin BIODUR™ E20. In order to keep the microvascular structure intact, the specimen was frozen for 24 h and afterwards the vessel walls were removed with a basic solution. BIODUR™ E20 is a two-component capillary–passable epoxy resin, which is used for contrast presentation of vessels. It stands out for great firmness and low inclination to shrinkage, less that 2%. The resin was colored by adding to the clear component EP20 red color EP21.

The absorption of the resin, at 532 nm, was measured experimentally. More specifically, a relative PA measurement was performed, and the PA signal of the resin was compared with that of an absorber with $\mu_a = 30\,\text{mm}^{-1}$. It was found that the epoxy has $\mu_a = 90\,\text{mm}^{-1}$, which is three times

TABLE I. Prime scattering coefficient of % Intralipid™ 10% solutions

Concentration % Intralipid™ 10%	μ_s' (mm^{-1})
0.0 (distilled water)	0.0
2.5	0.375
5.0	0.750
7.5	1.125
10.0	1.5

higher than that of the oxygenated blood at the above-mentioned wavelength.

Intralipid™ is a fat emulsion that is used clinically as an intravenously administered nutrient. It consists of water and phospholipid micelles, polydisperse in size. The fact that it is turbid and has low absorption bands in the visible region of the electromagnetic spectrum makes it a suitable phantom medium for simulating tissue optical properties.[14]

In the study of van Staveren *et al.*,[14] the absorption, scattering and anisotropy coefficients of Intralipid™ 10% have been measured for a range of wavelengths and have been compared with the calculated ones, which were based on Mie theory. They concluded that the scattering coefficient μ_s and the anisotropy coefficient g could be calculated as a function of the wavelength λ from their Eqs. (6.1) and (6.2) with an accuracy of ±6%:

$$\mu_s(\lambda) = 0.016\lambda^{-2.4}, \tag{2}$$

$$g(\lambda) = 1.1 - 0.58\lambda, \tag{3}$$

for $0.4 < \lambda < 1.1$, where λ is in micrometers and μ_s is in units of mm^{-1}/(ml/l). The calculated values hold for concentrations up to ~17% Intralipid™ 10% for 400 nm and 4% Intralipid™ 10% for 1100 nm.

Different values of the Intralipid™ coefficients have been reported in the literature, which are mainly attributed to the difference in the solution composition, in the particle size, and in the preparation procedure.[15–17] However, the properties of the Intralipid™ 10% suspensions that were used as tissue phantoms in the experiments, were calculated from the Eqs. (2) and (3).

For each depth five different Intralipid™ 10% dilutions were used. The reduced scattering coefficients of these solutions at 532 nm are summarized in Table I and have been calculated according to the properties of 10% Intralipid™ 10%.[15,18] The cast is shown in the Fig. 2 and the diameters of its branches for different positions are summarized in Table II.

The diameters of the vessels were measured with an optical microscope with an accuracy of ±10 μm. The diameters vary from 60 μm in the capillaries to 500–800 μm in the main artery. In the position of 4 mm (point A) the diameter is 625 μm, while in the position of 8 mm the fifth branch has a diameter of 300 μm (point B). These two points were used as reference points for evaluating the image resolution.

III. RESULTS AND DISCUSSION

The 3D images of the cast were calculated by using the beam forming algorithm and were visualized by using the
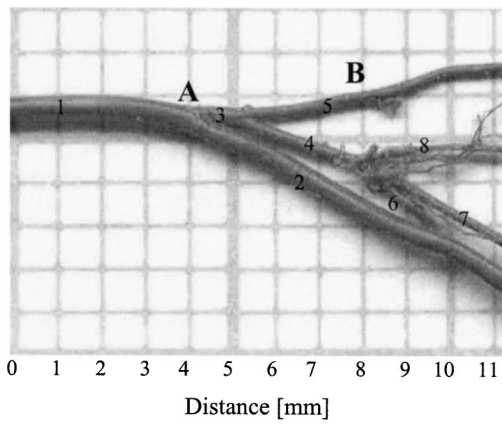
FIG. 2. Conjunction of the inferior and superior epigastric arteries of a Wistar rat, where the vascular cast branches are numbered from 1 to 8 as is indicated in Table II. Points A and B, where the vessel diameters are 625 and 300 μm, respectively, are used as reference points for evaluating the image resolution.

interactive data language (IDL®, Research System, Inc.). The IDL was chosen because it is a complete computing environment for interactive analysis and visualization of data. Moreover, IDL integrates a powerful array oriented language with numerous mathematical analyses and graphical display techniques that minimize the programing effort and time.

The imaging program uses the sensor coordinates at the detection plane, the recorded photoacoustic signals, and the sensor directivity as input data. The program does not correct for the diffuse photon flux caused by the Intralipid™ 10% dilutions, because the analytical form of it is not known. The boundaries of the image are determined by the area of the sensor array, although subimages can be calculated as well. The voxel size determines the image resolution, and in practice, cannot be smaller than the actual resolution of the sensor. Its size determines, also, the time window that is used in the program. At first, a structure with elements corresponding to the image voxels is created and initialized by setting its values to zero. Following, for each volume element to be imaged the acoustic transit time to each detector is calculated

TABLE II. Diameters (in μm) of the branches of the vascular cast.

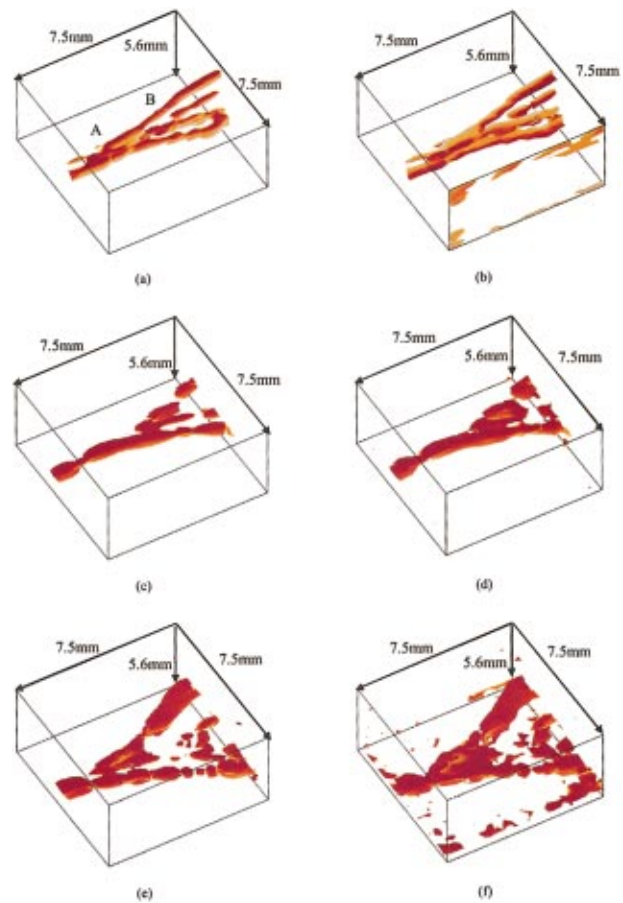| Distance (mm)	Vascular Cast Branches Diameter (μm)							
	1st	2nd	3rd	4th	5th	6th	7th	8th
0.0	500							
1.0	512							
2.0	512							
3.0	512							
4.0	625							
4.5	812							
5.0		500	375					
5.5		500	812					
6.0		500		337	275			
7.0		537		337	312			
8.0		562		500	312			
9.0		512			300	312	250	275
10.0		512			275		250	150
11.0		512			250		250	150

FIG. 3. (Color) 3D images of the vascular cast, where the medium and the scanning steps are: (a) water, 100 μm; (b) water 300 μm; (c) 5% Intralipid™ 10% 100 μm; (d) 5% Intralipid™ 10% 300 μm; (e) 10% Intralipid™ 10% 100 μm; and (f) 10% Intralipid™ 10% 300 μm.

and from that the time delays to be applied to these signals in order to construct a synthetic acoustic lens are calculated, also. Afterwards, for each focus point, the relevant signal part of each detector (time windowing) is added to the voxel value after it has been properly delayed and weighted. The beam former intensity in each voxel is derived from the focal arrays according to the peak-to-peak values of the signals.

In Fig. 3, the images of the branching of the epigastric artery system for three different dilutions, in the depth of 5 mm, are shown. The quality of the images depends on the system resolution, the scanning step, and the light distribution. The system resolution is a constant factor for all the measurements. As a result of that, the smaller structure that can be imaged is in order of 150 μm$\times$150 μm$\times$15 μm. PA sources, which can be detected, with smaller size, will be reconstructed as a voxel with the above dimensions. Due to "low" lateral resolution, the images of small structures suffer from blurring in the $x-y$ plane.

A relative big scanning step compared to the specimen size and the lateral resolution, will result in discontinuities, blurring, and roughness in the 3D images. That can be easily seen in all the images with a scanning step of 300 μm. In the presented series of experiments the number of measurement points, in the first case of 100 μm, is 5776, while in the second one it is 676, a factor of 8.5 lower.
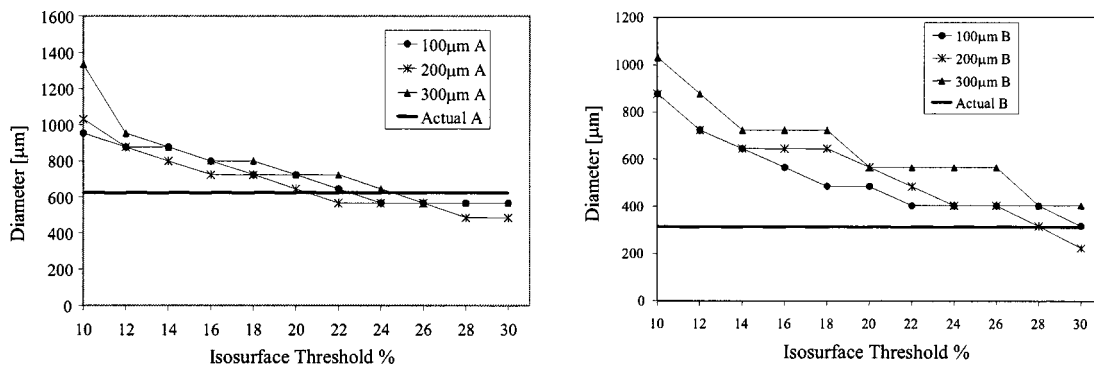
FIG. 4. Graphs of the vessel diameter at points A and B vs the isosurface threshold. Data are from measurements of the cast in water, at a depth of 5 mm and for scanning steps of 100, 200, and 300 μm. (a) Graph of the vessel diameter at point A, where the actual diameter is 625 μm. (b) Graph of the vessel diameter at point B where the actual diameter is 300 μm.

As was expected, the quality of images is in most cases relatively worse and the sample reconstruction is less satisfactory. Taking into account all the performed experiments, we can conclude that the scanning step should be at least equal to the lateral resolution if the structure size is in the region of 200 μm or smaller and can be increased for larger structures.

Another important parameter is the homogeneity of the light distribution around the specimen. That is related to the absorption and scattering coefficients of the surrounding medium. In order to study this effect, five different Intralipid™ 10% dilutions were used. The absorption coefficient of these dilutions can be neglected. In water ($\mu_s' = 0$), the laser beam remains focused and specific spots on the specimen are illuminated in each measurement point. That results in stronger PA signals, and by choosing an appropriate scanning step, the 3D constructed image [Fig. 3(a)] approaches the specimen satisfactorily. By increasing the μ_s', the light distribution becomes more homogenous and PA signals are generated from the whole cast. Thus, in a single measurement point, more signals are received, compared to the previous case.

In addition, the absorbed energy per area unit drops, but that can be easily anticipated by increasing the beam energy always with respect to the safety limits. The images in Figs. 3(c) and 3(e) are comparable with that of water. This is encouraging, since the dilution of 10% Intralipid™ 10% has similar scattering properties with real tissue. Thus, we expect to be able to image similar structures *in vivo*. Difficulties can be expected only in the case of larger scanning steps, as can be seen from the Figs. 3(b), 3(d), and 3(f), where the quality of the 3D images is relative low.

The constructed volumes are actually 3D isosurfaces of normalized data, which are plotted for a specific threshold. The data have been normalized to their maximum value and have been scaled from 0 to 255 in order to use pseudocolor for the graphical representation. Because of the normalization, different measurement sets cannot be compared in a quantitative way, after processing the data with the IDL program. That can be done only with the measured signals. The isosurface threshold can be determined using the histogram of the voxel values. The isosurfaces could be obtained with the same interval as the threshold values. The images, in Fig.

3, have been calculated by rejecting the isosurfaces with lower values than the threshold.

In order to evaluate the influence of the threshold value on the image resolution, the diameters at points A and B were calculated from the 3D volumes and were compared with the real ones. For this purpose, the data from the measurement of the cast in the water, at 5 mm with steps of 100, 200, and 300 μm were used. The images were calculated for thresholds of 10%–30% with an interval of 2%. Assuming Gaussian error distributions, the calculated diameters may be corrected for the sensor diameter, which defines the lateral resolution, according to the following error equation:

$$D_{\text{cor}}^2 = D_{\text{meas}}^2 - D_{\text{sens}}^2, \tag{4}$$

where D_{cor} is the corrected vessel diameter, D_{meas} id the diameter calculated from the 3D data, and D_{sen} is the diameter of the sensor, which is equal to 200 μm.

As can be seen from Fig. 4, large structures, as is the main artery, demand more isosurfaces in order to be reconstructed properly. Therefore, lower thresholds have to be applied. On the other hand, small structures, as is the fifth branch, can be reconstructed with a smaller number of isosurfaces and subsequently higher thresholds have to be used. The first case could result in blurring and "swelling" of the small objects, since not enough isosurfaces are drawn. The second case could lead to discontinuities and breaks of the objects, because of the low number of the isosurfaces that are plotted. The optimum threshold is dependent on the measured data set and the size of the scanning step relative to the specimen size.

In summary, it was shown that PA could be used for 3D imaging of small structures in turbid media, with depth resolution of 10–20 μm and lateral resolution of 100–200 μm. A depth of 7 mm can be reached with 532 nm light, which indicates that the system can be used for cutaneous medical applications. The lateral resolving power appears to be dependent on the way the 3D images are represented, which in turn depends on the setting of the isosurface threshold. The synthetic delay-and-sum beam forming algorithm works properly and the image quality can be improved with further processing (filtering, interpolation, etc.). Our purpose is to

improve the lateral resolution by constructing more-sensitive PA sensors and to proceed to real tissue measurements (animal experiments, patients).

[1] P. C. Beard and T. N. Mills, Phys. Med. Biol. **42**, 177 (1997).

[2] R. O. Esenaliev, A. A. Karabutov, F. K. Tittel, and A. A. Oraevsky, Proc. SPIE **2979**, 71 (1997).

[3] M. C. Pilatou, R. I. Siphanto, L. N. A. van Adrichem, and F. F. M. de Mul, Rev. Sci. Instrum. **74**, 384 (2003).

[4] C. G. A. Hoelen, F. F. M. de Mul, R. Pongers, and A. Dekker, Opt. Lett. **23**, 648 (1998).

[5] C. G. A. Hoelen and F. F. M. de Mul, J. Acoust. Soc. Am. **106**, 695 (1999).

[6] C. G. A. Hoelen, A. Dekker, and F. F. M. de Mul, IEEE Trans. Ultrason. Ferroelectr. Freq. Control **48**, 37 (2001).

[7] C. G. A. Hoelen and F. F. M. de Mul, Appl. Opt. **39**, 5872 (2000).

[8] M. W. Sigrist and F. K. Kneubuhl, J. Acoust. Soc. Am. **64**, 1652 (1978).

[9] D. A. Hutchins, Can. J. Phys. **64**, 1247 (1986).

[10] A. C. Tam, Rev. Mod. Phys. **58**, 381 (1986).

[11] D. H. Johnson and D. E. Dudgeon, *Beamforming in Array Signal Processing: Concepts and Techniques*, 1st ed. (PTR Prentice-Hall, Englewood Cliffs, NJ, 1993), Vol. 1, Chap. 4, p. 111.

[12] C. G. A. Hoelen, *3D Photoacoustic Tissue Imaging: Towards Noninvasive Medical Photoacoustic Diagnosis*, 1st ed. (University of Twente, Enschede, 1998), Vol. 1, Chap. 5, p. 126.

[13] A. A. Karabutov, E. V. Savateeva, N. B. Podymova, and A. A. Oraevsky, J. Appl. Phys. **8**, 2003 (2000).

[14] S. T. Flock, S. L. Jacques, B. C. Wilson, W. M. Star, and M. J. C. van Gemert, Lasers Surg. Med. **12**, 510 (1992).

[15] H. J. Staveren, C. J. M. Moes, J. van Marle, S. A. Prahl, and M. J. C. Gemert, Appl. Opt. **30**, 4507 (1991).

[16] C. J. Moes, M. J. van Gemert, J. P. A. Marijnissen, and S. A. Prahl, Appl. Opt. **28**, 2292 (1989).

[17] W. M. Star, J. P. A. Marijnissen, H. Hansen, M. Keijzer, and M. J. C. van Gemert, Photochem. Photobiol. **46**, 619 (1987).

[18] I. Driver, J. W. Feather, and J. B. Dawson, Phys. Med. Biol. **34**, 1927 (1989).